Article

Discovery Medicine 2025; 37(200): 1874–1884
https://doi.org/10.24976/Discov.Med.202537200.162

A Prognostic Model for Acute Myeloid Leukemia Based on Immunogenic Cell Death-Related Genes

Guocai Li[1], Yaqin Gong[2,*]

[1]Department of Blood Transfusion, The Third Xiangya Hospital of Central South University, 410013 Changsha, Hunan, China
[2]Department of Traditional Chinese Medicine, The Third Xiangya Hospital of Central South University, 410013 Changsha, Hunan, China
*Correspondence: gyq170327@163.com (Yaqin Gong)
Submitted: 20 May 2025 Revised: 23 July 2025 Accepted: 21 August 2025 Published: 20 September 2025

Background: Immunogenic cell death (ICD) has emerged as a key factor in cancer prognosis; however, its application in prognostic modeling for acute myeloid leukemia (AML) remains unexplored. Therefore, this study aimed to develop a prognostic model for AML based on ICD-related genes.
Methods: ICD-related genes exhibiting differential expression in AML were identified from The Cancer Genome Atlas (TCGA) database. Initially, candidate genes were filtered using univariate cox proportional hazards model (Cox) and least absolute shrinkage and selection operator (LASSO) Cox regression analyses before being incorporated into a prognostic model. An ICD-related gene signature was then established via the survival package. Furthermore, immune cell infiltration was evaluated using Estimation of STromal and Immune cells in MAlignant Tumor tissues using Expression data (ESTIMATE), immunedeconv, and ggstatsplot.
Results: Of the total 34 ICD-related genes, 27 demonstrated differential expression, with five genes correlating with AML prognosis. By LASSO regression, we identified four ICD-related genes, including cluster of differentiation 4 (CD4), interleukin-10 (IL10), caspase-1 (CASP1), and phosphatidylinositol-4,5-bisphosphate 3-kinase catalytic subunit alpha (PIK3CA). Increased risk scores in our model were indicative of a poorer prognosis in AML patients ($p < 0.001$). Time-dependent Receiver Operating Characteristic (ROC) analysis demonstrated strong predictive capability, with overall survival rates of 0.709, 0.650, and 0.768 at 1, 3, and 5 years, respectively. Nomogram calibration curves confirmed its predictive accuracy. Furthermore, risk scores were substantially correlated with immune cell infiltration ($p < 0.05$). Moreover, suppression of CASP1 expression significantly diminished AML cell proliferation and increased their sensitivity to chemotherapeutic agents *in vitro* ($p < 0.01$).
Conclusion: This study developed a prognostic model for AML using four ICD-related genes (*CD4*, *IL10*, *CASP1*, and *PIK3CA*). This model demonstrates good predictive accuracy and shows close association with immune infiltration, consistent with functional verification results *in vitro*, underscoring its potential utility in prognosis assessment and therapeutic decision-making.

Keywords: acute myeloid leukemia; prognostic model; LASSO regression; immuno-infiltration; prognostic biomarkers; survival prediction

Introduction

Acute myeloid leukemia (AML) represents a prevalent hematologic malignancy affecting the bone marrow and blood cells [1]. Chemotherapy remains the standard treatment option for AML, aiming to eliminate malignant cells and restore normal hematopoiesis. In certain cases, hematopoietic stem cell transplantation may be required. Although AML remains a challenging disease, recent advances in chemotherapy regimens and bone marrow transplantation have improved patient outcomes [2].

The prognosis of AML varies across patients and is influenced by factors like disease subtype, patient age, comorbidities, and the presence of high-risk gene mutations. Current research on prognostic models for AML has integrated various sets of genes, such as those related to ferroptosis and pyroptosis, to predict patient outcomes by combining clinical and genomic features [3,4]. These models incorporate factors such as age, disease subtype, genetic mutations, and treatment response to provide personalized risk assessments and inform treatment decisions [5]. However, further investigations are required to refine and validate these models, thereby enhancing prognostic accuracy and improving patient outcomes.

Immunogenic cell death (ICD) is a type of regulated cell death that triggers an adaptive immune response against cancer [6]. Recently, ICD has been proposed to serve as a predictive biomarker for cancer treatment outcomes [7]. Tumor prognostic models incorporating ICD rely on markers such as calreticulin exposure, ATP release, and high mobility group box 1 (HMGB1) production to predict patient prognostic outcomes. Elevated levels of these ICD markers have been linked to improved overall survival and enhanced treatment response in various cancer types, sug-

gesting their potential to guide personalized therapeutic approaches [8,9]. A recent study demonstrated that an ICD risk signature (ICDRS) improves European Leukemia Net (ELN) risk stratification in AML and predicts immune infiltration landscapes [10]. However, to the best of our knowledge, no prognostic model based on ICD-related genes has been established for AML. In AML, ICD can activate immune responses that modulate leukemic cell proliferation, apoptosis, and drug resistance by engaging immune cells within the bone marrow microenvironment, making ICD-related genes as promising prognostic markers [11,12].

This study aimed to establish a prognostic signature for AML patients built on ICD-associated genes. Functional analysis further confirmed the role of Caspase-1 (CASP1) in AML cell biology, supporting its candidacy as a therapeutic target. Additionally, we explored the prognostic significance of ICD-related genes and their links to clinical features, highlighting their potential as novel biomarkers and candidates for targeted treatment.

Materials and Methods

Assessing Differential Expression of ICD-Related Genes

RNA sequencing data for AML and ordinary samples, uniformly processed by the Toil pipeline, were retrieved from The Cancer Genome Atlas (TCGA, https://portal.gdc.cancer.gov, v37.0) and Genotype-Tissue Expression (GTEx, https://www.gtexportal.org/home/, v8) [13]. Raw expression values were transformed by $\log_2$(value+1). Clinical and prognostic data for AML patients were obtained from TCGA. Differential expression of ICD-related genes between AML and normal tissues was analyzed using the NetworkAnalyst (https://www.networkanalyst.ca/). Finally, 34 ICD-related genes were selected following a previous study that compiled pre-clinically validated ICD markers, which are critical for eliciting antitumor immunity via pathways such as calreticulin exposure and HMGB1 release [14].

These genes, previously correlated with immune activation and prognostic relevance in solid tumors, were selected to explore their role in AML, whereas the prognostic and therapeutic potential of ICD, including necroptosis-driven immunity, remains largely underexplored [15,16]. Expression patterns of ICD-related genes were illustrated using the R package ComplexHeatmap (v2.13.1; Bioconductor, Seattle, WA, USA). Statistically significant differentially expressed ICDs were visualized using the ggplot2 package. Differentially expressed ICD-related genes were further examined for protein-protein interactions (PPIs) using Search Tool for the Retrieval of Interacting Genes (STRING) (https://string-db.org/, v11.5; interaction score $\geq$0.4), and the interaction network was constructed and visualized in Cytoscape (v3.9.1). Gene mutation profiles were obtained from cBioPortal (http://www.cbioportal.org/).

Identification of Prognostic Genes

To evaluate the association between ICD gene expression and overall survival (OS) in AML patients, univariate cox proportional hazards model (Cox) regression was conducted using the survival package (v3.3.1), and genes with $p < 0.05$ were included in further analysis. To address gene collinearity, least absolute shrinkage and selection operator (LASSO) Cox regression was employed, with ten-fold cross-validation used to determine the lambda value. The deviance corresponding to each lambda value (penalty term) during the LASSO coefficient screening process was visualized, facilitating the development of a prognostic model.

Establishment of an ICD Gene-Based Prognostic Signature

Multivariate Cox regression was conducted using the survival package (v3.3.1) to calculate a risk score for each participant. Based on the median risk score, patients were classified into high- and low-risk groups. The OS rate was compared between these groups and visualized using ggplot2 (v3.3.6). Proportional hazard assumptions were examined using survival and ggplot2, and survival curves were drawn using survminer.

Nomogram Construction and Calibration Curves

Cox regression and proportional hazards assumption tests were conducted using the survival package (v3.3.1). Nomograms were developed and visualized with the rms package (v6.3-0), and calibration curves were subsequently plotted to estimate 1-, 2-, and 3-year survival rates in AML patients.

Immuno-Infiltration Analysis

Matrix and immune scores corresponding to the cloud data were calculated using the estimate R package (v1.0.13) [17]. The immunedeconv R package was employed to assess immune cell infiltration, while ggstatsplot was used to visualize correlations between risk score and immune score. Spearman's rank correlation was applied for non-parametric data, with significance defined at $p < 0.05$.

Cell Culture

HL-60 and THP-1 cells were sourced from the Chinese Academy of Sciences Cell Bank (Shanghai, China), which provides cell lines authenticated by short tandem repeat (STR) profiling. Moreover, mycoplasma contamination was examined in both cell lines using a quantitative polymerase chain reaction (qPCR)-based assay, and the results confirmed their contamination-free status (**Supplementary Table 1**). Cells were cultured in RPMI-1640 medium (Hyclone, Logan, UT, USA, SH30027.01) containing 10% fetal bovine serum (FBS) (Life Technologies, Carlsbad, CA, USA, 10099-141), and were transfected

with siRNA or control siRNA (siNC; CAT#: R10043, Ribobio, Guangzhou, China) using Lipofectamine 2000 (Invitrogen, Waltham, MA, USA, 11668019) following the manufacturer's guidelines. The CASP1 siRNA sequences were as follows: 5′-GCCCAAGUUUGAAGGACAATT-3′ (sense), 5′-UUGUCCUUCAAACUUGGGCTT-3′ (antisense).

qPCR

Total RNA was extracted from HL-60 and THP-1 cells using Total RNA Isolation reagent (TRIzol) reagent (Invitrogen, Waltham, MA, USA, Cat# 15596026) following the manufacturer's instructions. Complementary DNA (cDNA) was synthesized using the PrimeScript RT Reagent Kit (Takara, Japan, Cat# RR037A). Quantitative PCR (qPCR) was performed using PowerUp SYBR Green Master Mix (Applied Biosystems, USA, Cat# A25742) on an ABI 7500 Real-Time PCR System (Applied Biosystems, USA, Model# 7500). Thermal cycling conditions consisted of an initial denaturation at 95 °C for 10 minutes, followed by 40 cycles of 95 °C for 15 seconds and 60 °C for 1 minute. CASP1 expression levels were normalized to glyceraldehyde-3-phosphate dehydrogenase (GAPDH) as an internal control using the $2^{-\Delta\Delta Ct}$ method. Primer sequences used in qPCR were as follows: 5′-GAAGGTGAAGGTCGGAGTC-3′ (forward) and 5′-GAAGATGGTGATGGGATTTC-3′ (reverse). CASP1 qPCR primer sequences were as follows: 5′-GAGAAACATCCAAAAGTGAGGG-3′ (forward), 5′-GCCTTTCTTCTGGTCAGTGC-3′ (reverse) [18].

Proliferation Assay

Cells (HL-60 or THP-1) were seeded in 6-well plates at a density of 2×10^5 cells per well and treated with cytarabine (Ara-C, 1 µM) for 48 hours. EdU (10 µM, Click-iT EdU Alexa Fluor 488 Imaging Kit, Thermo Fisher, USA) was added 2 hours before fixation. Cells were then fixed with paraformaldehyde, permeabilized with 0.5% Triton X-100, and fluorescently labeled with Click-iT 488-azide for 30 minutes in the dark. In the next step, cell nuclei were counterstained with 1 µg/mL DAPI for 10 minutes. Finally, proliferation rates were quantified using fluorescence-activated cell sorting (FACSDiva) (BD Biosciences) on an LSRII flow cytometer (BD Biosciences, San Jose, CA, USA; Model: LSR II), and EdU-positive cells were analyzed via FlowJo (v10.8.1).

Western Blotting Analysis

Western blotting was conducted using standard experimental protocols. Briefly, total proteins were isolated from the cells, resolved through sodium dodecyl sulfate–polyacrylamide gel electrophoresis (SDS-PAGE), and subsequently transferred onto polyvinylidene fluoride (PVDF) membranes. Membranes underwent overnight incubation with primary antibodies (Abcam plc; Cambridge, MA, UK) targeting CASP1 (Abcam, ab179515, 1:1000), BCL2–associated X protein (BAX) (Abcam, ab32503, 1:1000), apoptosis regulator BAX (BCL2) (Abcam, ab32124, 1:1000), Caspase-3 (Cell Signaling Technology, #9661, 1:1000 dilution), and GAPDH (rabbit, Abcam, ab9485, 1:2000). The following day, membranes were thoroughly washed and incubated with goat anti-rabbit IgG secondary antibodies (7074S, 1:5000, Cell Signaling Technology, Danvers, MA, USA). Protein bands were then visualized using an enhanced chemiluminescence (ECL) detection system (Thermo Fisher Scientific, 34580), and band intensities were measured using ImageJ software (version 1.53, National Institutes of Health, Bethesda, MD, USA). Protein bands were normalized to GAPDH as a loading control.

Statistical Analysis

Basic mathematical analysis and processing were performed in MS Excel software (version 2019, Microsoft Corporation, Redmond, WA, USA). All major analyses and visualizations were made using R (v4.0.3, Austria). Each finding was verified through three independent experiments. Data following a normal distribution were expressed as mean ± SD, while non-normally distributed data were presented as median (interquartile range). For non-parametric data, statistical comparisons between two groups were performed using the Wilcoxon or Mann–Whitney U test. For multiple-group comparisons, one-way ANOVA followed by Tukey's post-hoc test was used for normally distributed data. Moreover, the Kruskal-Wallis test with Dunn's post-hoc test was used for non-parametric data. All experiments were conducted in triplicate (n = 3), and a p-value of <0.05 was regarded as statistically significant.

Results

Differential Expression Analysis of ICD-Related Genes in AML

We analyzed data from 173 AML patients (TCGA) and 70 normal samples (GTEx). A total of 34 ICD-related genes, as identified by Garg *et al.* [14], were examined and visualized using a heatmap (**Supplementary Fig. 1a**). Of these, 27 were significantly differentially expressed (**Supplementary Fig. 1b**). The PPI interactions and mutation distributions are displayed in **Supplementary Fig. 1c,d**, respectively.

Screening for Prognostic ICD-Related Genes

Univariate Cox analysis identified 5 significant genes ($p < 0.05$), including potential risk genes (*CD4*, *IL10*, *CASP1*, *IFNGR1*) and 1 potential protective gene (PIK3CA) (Fig. 1a). To develop the ICD-based prognostic model, LASSO regression was applied to these five genes (*CD4*, *IL10*, *CASP1*, *PIK3CA*, and *IFNGR1*), filtering out

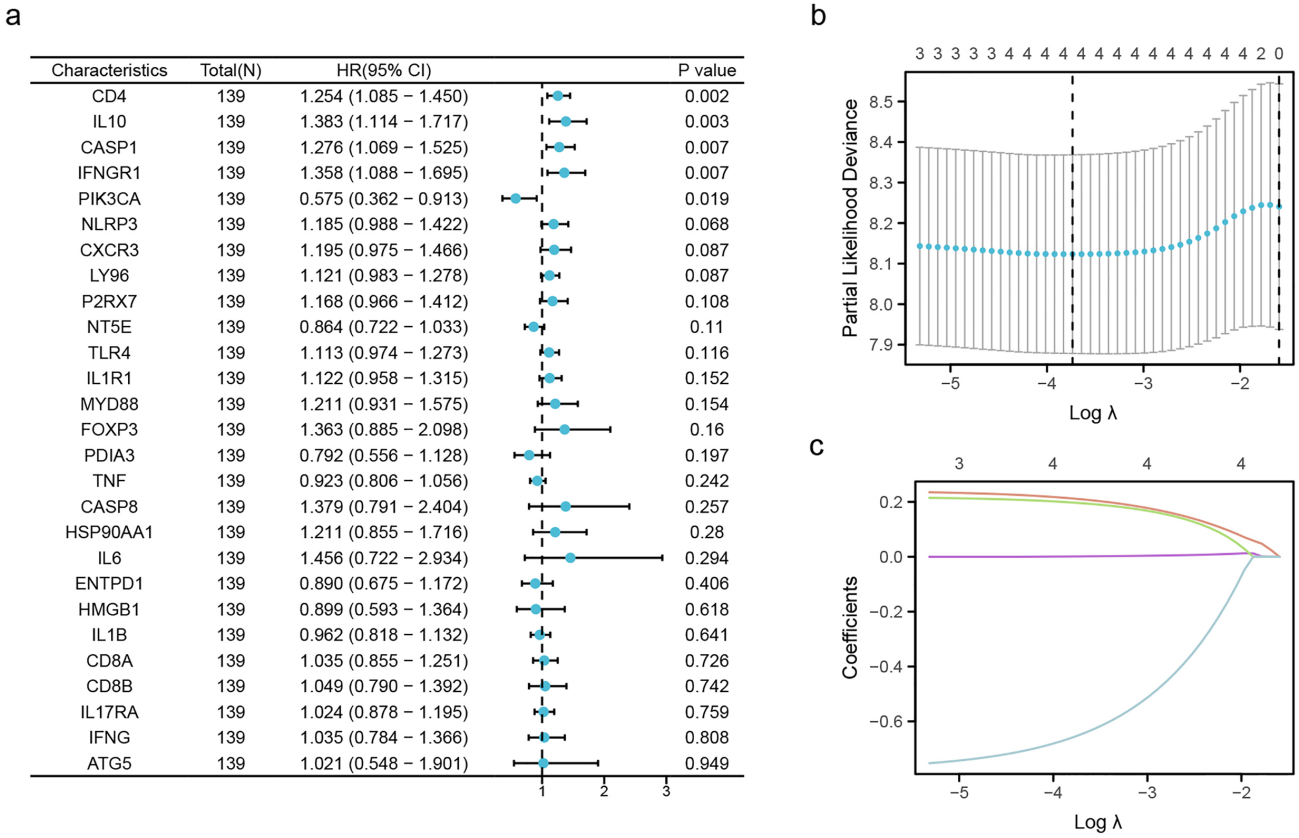

Fig. 1. Screening for prognostic ICD-related genes. (a) Univariate Cox regression of 27 differentially expressed ICD-related genes, identifying five genes (*CD4*, *IL10*, *CASP1*, *IFNGR1*, *PIK3CA*) with $p < 0.05$. (b) LASSO regression filtered out variables with coefficients of zero through cross-validation to select optimal lambda values, reducing the gene set to four (*CD4*, *IL10*, *CASP1*, *PIK3CA*) based on non-zero coefficients, which were assigned weights in the prognostic model to calculate risk scores (*CD4*: 0.12, *IL10*: 0.08, *CASP1*: 0.15, *PIK3CA*: –0.10). (c) LASSO variable locus diagram, showing the trajectory of coefficient shrinkage for the selected genes. ICD, Immunogenic cell death; LASSO, least absolute shrinkage and selection operator.

variables with coefficients of zero corresponding to lambda values (Fig. 1b). Ten-fold cross-validation identified an optimal lambda value of 0.023864 (index = 24), yielding the lowest average cross-validation error, a deviance of 8.1234, and a standard error (SE) of 0.24491, with four non-zero coefficients. Finally, four ICD-related genes, including *CD4*, *IL10*, *CASP1*, and *PIK3CA*, were selected for the prognostic model (Fig. 1c).

Construction of a Prognostic Model Using ICD-Related Genes in AML

A prognostic model was developed based on 4 ICD-related genes (*CD4*, *IL10*, *CASP1*, and *PIK3CA*), with the following risk score formula:

Risk score = (0.068 × *CD4*) + (0.160 × *IL10*) + (0.162 × *CASP1*) – (0.630 × *PIK3CA*).

AML patients were stratified into high- and low-risk groups, with the median risk score as the threshold. Higher risk scores were associated with worse prognosis in AML patients. Notably, *CD4*, *IL10*, and *CASP1* were upregulated and PIK3CA was downregulated in the high-risk group (Fig. 2A). Kaplan-Meier curves revealed that patients in the high-risk group have substantially poorer prognosis. The log-rank test confirmed a statistically significant difference, yielding HR = 2.018 (95% CI: 1.321–3.083; $p = 0.0009$) (Fig. 2B, **Supplementary Table 2**). Time-dependent ROC analysis demonstrated prognostic accuracies for OS of 0.709 (95% CI: 0.6177–0.7994) at 1 year, 0.650 (95% CI: 0.5405–0.7587) at 3 years, and 0.768 (95% CI: 0.6269–0.9089) at 5 years (Fig. 2C).

Construction of Nomogram and Calibration Curves

We developed a nomogram that integrates age, gender, cytogenetic risk, and risk score to provide a better quantitative method for predicting the prognosis of AML patients. The nomogram showed that the risk score was a crucial factor among various clinical parameters (Fig. 3a). Calibration analyses verified the nomogram's accuracy in forecasting AML patient outcomes (Fig. 3b–d). For comparative assessment, we specifically used the European LeukemiaNet (ELN) 2017 classification system [19], which is a widely adopted AML risk stratification framework. Our model

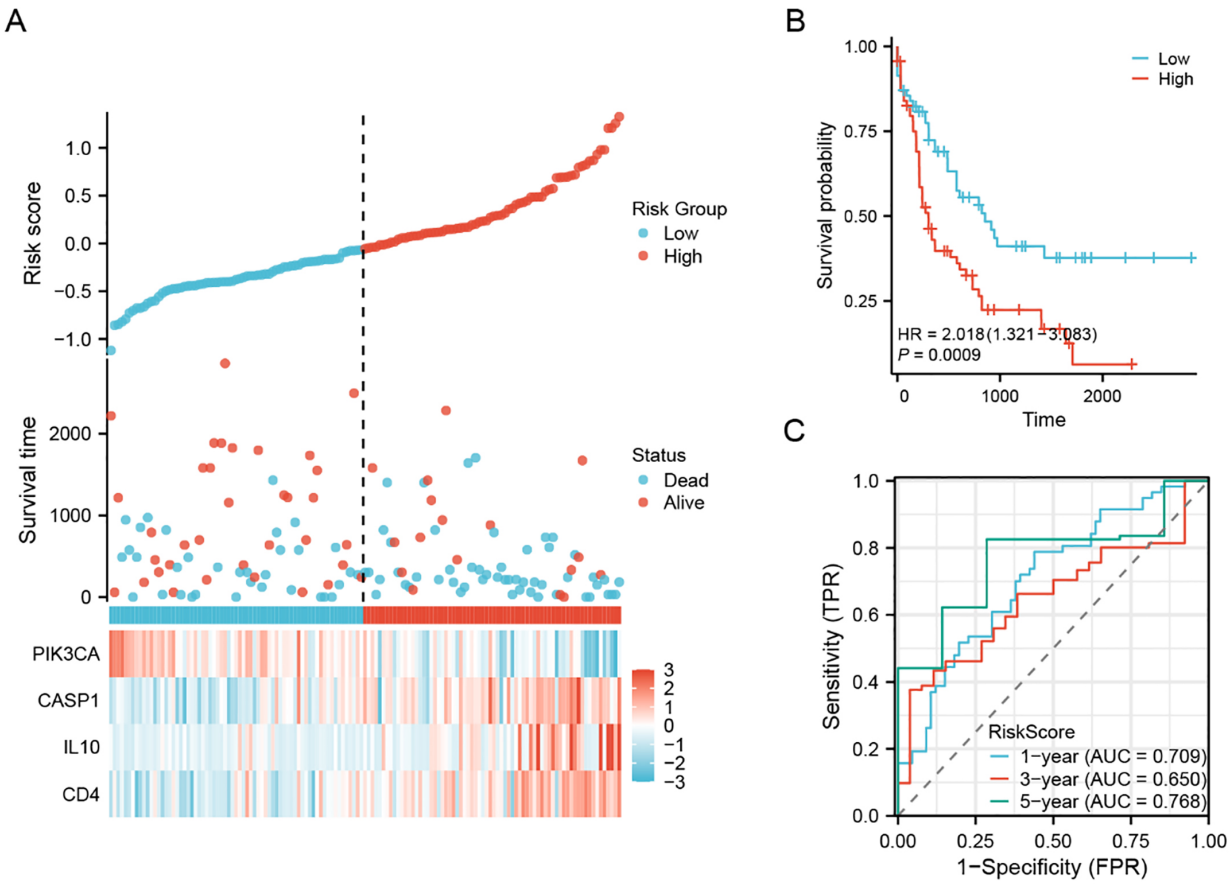

Fig. 2. Construction of a prognostic model based on ICD-related genes. (A) The top scatterplot displays risk scores arranged in ascending order, illustrating the relationship between risk score, survival time, and status across samples. The bottom heatmap depicts the signature's gene expression. (B) Kaplan–Meier survival estimation for stratified risk groups. (C) ROC-based assessment of the risk score's prognostic value. ROC, Receiver Operating Characteristic.

demonstrated a similar Area Under Curve (AUC), indicating its predictive accuracy (Fig. 3e).

Immuno-Infiltration Analysis

We analyzed specific immune cell types, including macrophage M2, monocyte, neutrophil, NK cells, and Tregs, owing to their pivotal roles in the AML tumor microenvironment. M2 macrophages and monocytes often promote AML progression by fostering immunosuppression and supporting tumor cell survival, whereas neutrophils can facilitate tumor growth via inflammatory signaling. Conversely, NK cells and Tregs are crucial to antitumor immunity, with NK cells driving cytotoxic responses and Tregs modulating immune suppression [20–22].

Relative to the low-risk group, the high-risk group had elevated infiltration of M2 macrophages, monocytes, and neutrophils, accompanied by reduced levels of NK cells and Tregs ($p < 0.05$, **Supplementary Fig. 2a**). Each of the four ICD-related genes showed a strong correlation with immune cell infiltration ($p < 0.05$, **Supplementary Fig. 2b–e**). Further analysis revealed that *CASP1*, *CD4*, and *IL10* exhibited significant associations with stromal, immune, and ESTIMATE scores ($p < 0.05$, **Supplementary Fig. 3a–d**). The risk score was found to be inversely correlated with B cells, NK cells, Tregs, and myeloid dendritic cells, and positively correlated with M2 macrophage and monocyte levels ($p < 0.05$, **Supplementary Fig. 4a–k**).

Given the significant correlation between CASP1 expression and immune cell infiltration, particularly its association with pro-tumorigenic immune cells like M2 macrophages, we investigated its functional role in AML cell proliferation and drug sensitivity through *in vitro* experiments to validate its therapeutic potential.

Functional Experiments In Vitro

To investigate the functional role of CASP1 in leukemia cell apoptosis, its expression was silenced in HL-60 and THP-1 cell lines using siRNA (Fig. 4a, $p < 0.05$) and the expression levels of apoptosis-related proteins was evaluated through Western blot analysis. CASP1 knockdown reduced the anti-apoptotic protein BCL2 and elevated the pro-apoptotic protein BAX (Fig. 4b–f) expressions, suggesting that CASP1 may modulate apoptotic through the BAX/BCL2 pathway. Notably, cleaved Caspase-3 expres-

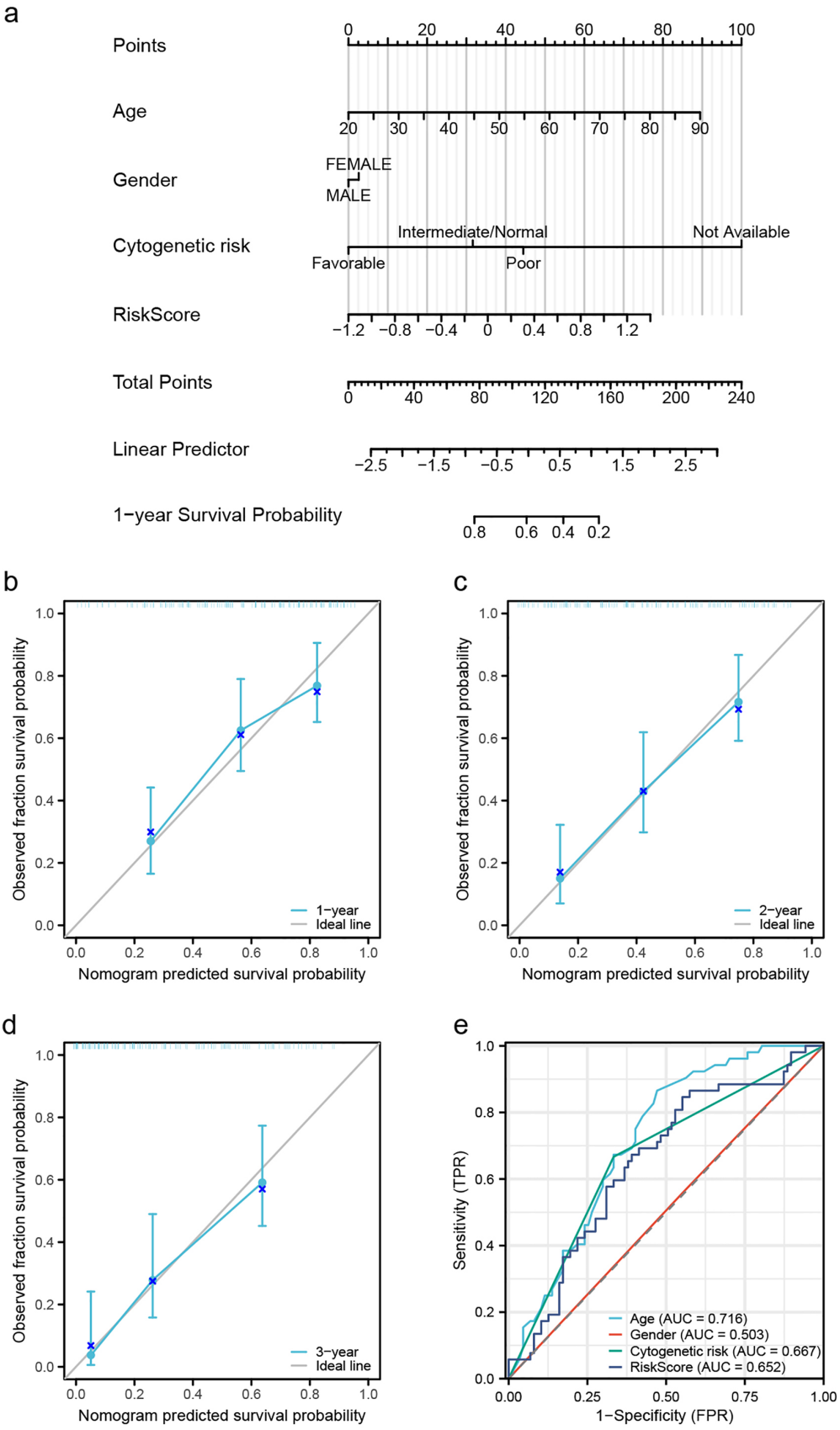

Fig. 3. Construction of the nomogram and calibration curves. (a) Nomogram combining age, gender, Cytogenetic risk, and risk score for forecasting the prognosis of AML patients. (b–d) Calibration curves of the nomogram. (e) AUC value of our model compared with others. AML, acute myeloid leukemia; AUC, Area Under Curve.

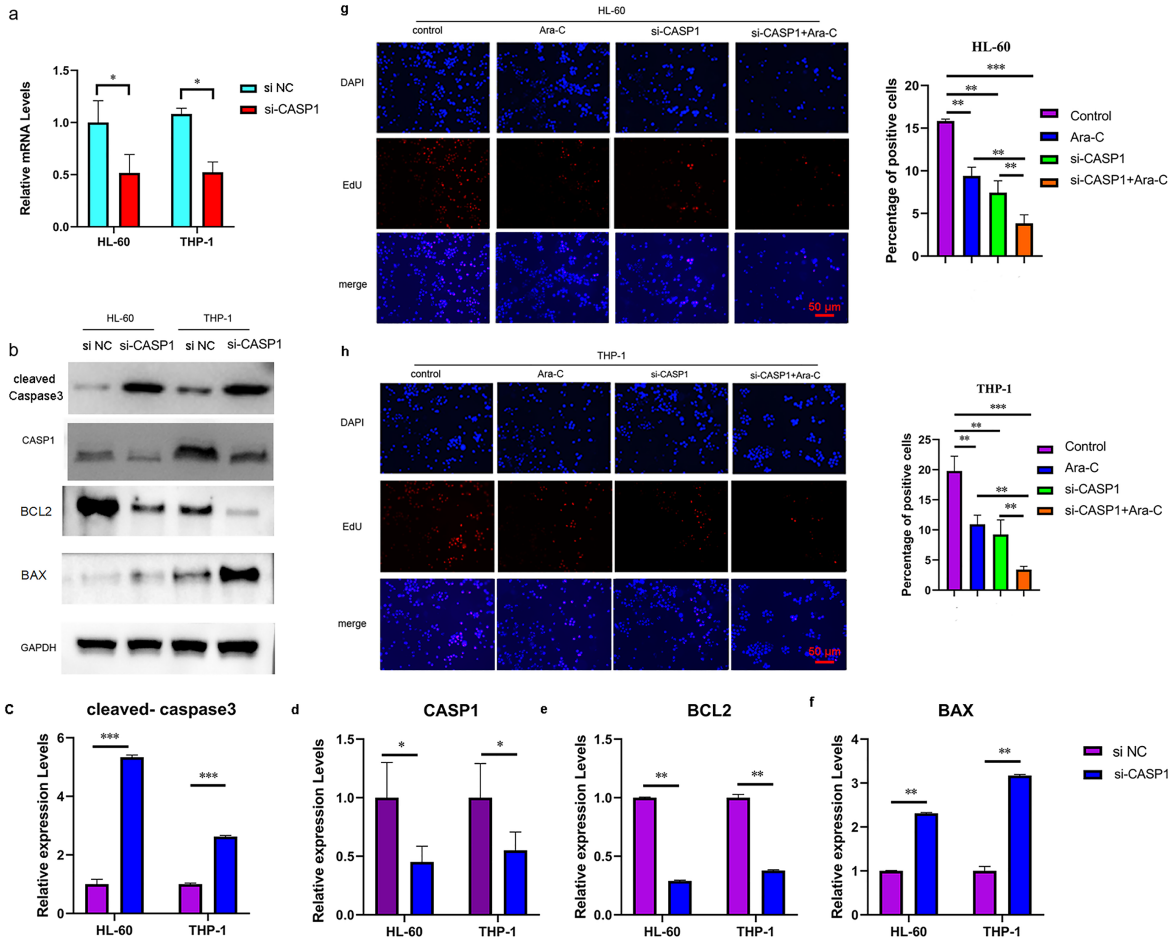

Fig. 4. Functional experiments *in vitro*. (a) The transfection efficiency of siRNA was assessed using qPCR. (b) Western blot analysis showing the expression of Caspase-3, CASP1, BCL2, and BAX after CASP1 silencing. (c–f) Quantitative analysis of protein expression levels: (c) cleaved Caspase-3, (d) CASP1, (e) BCL2, and (f) BAX, normalized to GAPDH. (g) Inhibition of CASP1 resulting in significantly increased sensitivity to cytarabine in HL-60 cells. (h) Inhibition of CASP1 resulting in significantly increased sensitivity to cytarabine in THP-1 cells. Data are expressed as mean ± SD, n = 3. $*p < 0.05$, $**p < 0.01$, $***p < 0.001$. Scale bars = 50 μm. qPCR, quantitative polymerase chain reaction; BCL2, B-cell lymphoma 2; BAX, BCL2–associated X protein; GAPDH, glyceraldehyde-3-phosphate dehydrogenase.

sion was significantly increased following CASP1 knockdown (Fig. 4b–f), indicating enhanced activation of the apoptotic cascade. Furthermore, while individual treatments with either Ara-C or si-CASP1 alone effectively suppressed proliferation in both HL-60 and THP-1 cells, their combined treatment yielded a more pronounced inhibitory effect. EdU proliferation assays revealed that proliferation rates in the combination group were significantly lower than in either single treatment group ($p < 0.01$, Fig. 4g,h).

To further explore the role of CASP1 in Ara-C–induced apoptosis, we performed Western blot analyses to assess the expression of apoptosis-related proteins following CASP1 knockdown. As illustrated in Fig. 5, Ara-C treatment decreased CASP1 and BCL2 levels while elevating BAX and cleaved Caspase-3 expression. A similar trend was observed with si-CASP1 treatment alone. However, combination treatment further enhanced these effects, resulting in pronounced suppression of CASP1 and BCL2 and upregulation of BAX and cleaved Caspase-3 ($p < 0.01$).

Collectively, these findings suggest that CASP1 may exert an anti-apoptotic function by regulating the BAX/BCL2 pathway and activating cleaved Caspase-3. Silencing CASP1 notably enhances Ara-C-induced apoptosis, emphasizing its importance in leukemia cell survival. These results highlight CASP1 as a potential molecular target for future leukemia treatments, suggesting that its inhibition could enhance the efficacy of chemotherapeutic drugs.

Discussion

These models help guide clinical management in AML and provide patients with precise prognostic information. Current prognostic models categorize patients into

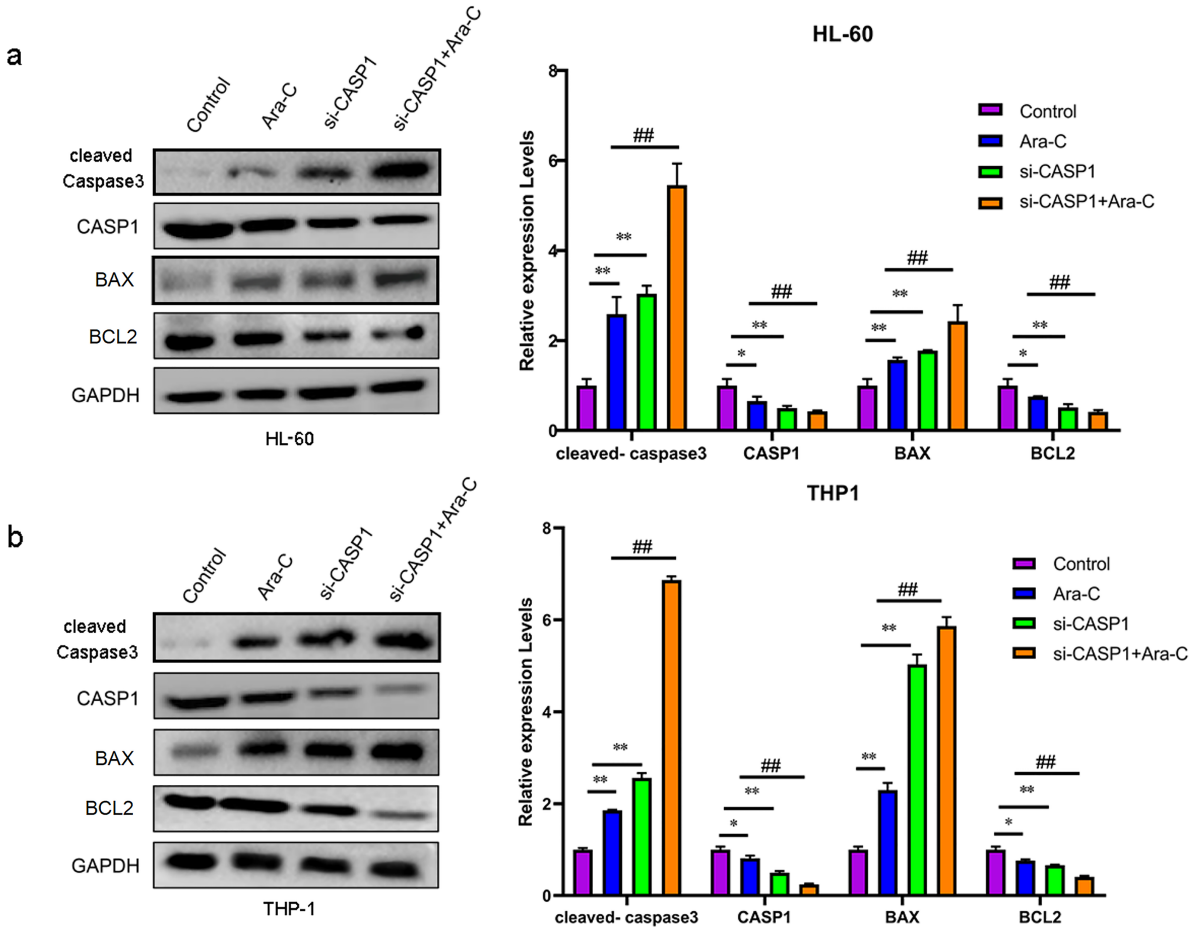

Fig. 5. Western blot analysis of cleaved Caspase-3, CASP1, BAX, and BCL2 expression. (a) HL-60 cells; (b) THP-1 cells. Quantitative analysis based on GAPDH normalization is illustrated in the bar graphs. Data are expressed as mean ± SD, n = 3. *$p < 0.05$, **$p < 0.01$ vs. control; $^{\#\#}p < 0.01$ vs. Ara-C or si-CASP1.

different risk groups based on cytogenetic, molecular, and clinical parameters. However, the inherent heterogeneity of AML, limited data, and time-dependent variables can hinder the predictive accuracy of these models [23]. Prediction models based on larger datasets, such as those from the TCGA database, may partially overcome these limitations. Although prognostic models based on ferroptosis, oxidative stress, and immune-related genes have been reported, there are no AML prognostic models constructed using ICD-related genes [3,24,25].

ICD-related gene-based prognostic models have shown clinical significance in several cancer types. For example, Min K *et al.* [26] constructed a five-gene model—BMP and activin membrane-bound inhibitor (BAMBI), transmembrane and coiled-coil domains 2 (TMCC2), NADPH oxidase 4 (NOX4), dickkopf wnt signaling pathway inhibitor 1 (DKK1), and cystathionine-β-synthase (CBS)—to predict outcomes in osteosarcoma. Another study utilized six ICD-related genes—calreticulin (CALR), C-type lectin domain containing 9a (CLEC9A), BAX, toll-like receptor 4 (TLR4), C-X-C motif chemokine receptor 3 (CXCR3), and PIK3CA—to construct a breast cancer prognostic model [9]. Fu *et al.* [27] established a four-gene ICD-based model and explored its correlation with immunotherapy response. Like these studies, we identified a notable correlation between ICD-related gene expression and AML prognosis, and established a prognostic model incorporating *CD4*, *IL10*, *CASP1*, and *PIK3CA*.

Earlier research has highlighted the roles of *CD4*, *IL10*, and *PIK3CA* in AML progression and prognosis [28–30]. In contrast, only one study has reported CASP1 as a marker of poor prognosis in AML patients [31]. Emerging evidence suggested that CASP1 is involved in regulating both chemoresistance and proliferation in solid tumor cells [32]. Our experimental data revealed that silencing CASP1 suppresses AML cell growth and enhances chemosensitivity, supporting its therapeutic relevance. However, the lack of *in vivo* validation limits the strength of these findings, and further investigations, including *in vivo* experiments using CASP1 inhibitors, are warranted to confirm its thera-

peutic efficacy in AML. Consistent with previous findings, our study demonstrated that CASP1 regulates both proliferation and drug resistance in AML cells under *in vitro* conditions. The concentration of Ara-C (8 μM) used in our study was carefully selected to balance therapeutic efficacy and mechanistic clarity. This dose aligns with clinically relevant concentrations that induce apoptosis in AML cells without causing excessive cytotoxicity, allowing precise assessment of CASP1's modulatory effect [33].

Our study demonstrated that the expression of *CD4*, *IL10*, *CASP1*, and *PIK3CA* significantly influences AML prognosis through distinct biological mechanisms. CD4+ T-cell activity is crucial for anti-leukemic immunity, and resistant AML cells exhibit impaired T-cell engagement, associated with poor survival outcomes [34]. IL10 signaling through IL-10R promotes leukemia stemness, and its overexpression correlates with disease progression, making it a promising target for CAR-T therapy [35]. Overexpression of CASP1 in AML drives poor prognosis by regulating inflammatory apoptosis pathways and enhancing leukemia cell proliferation [31]. PIK3CA-mediated phosphoinositide 3-kinase (PI3K)/AKT serine/threonine kinase (AKT) signaling promotes leukemogenesis, with isoform-specific dysregulation contributing to therapy resistance [36]. Collectively, these genes modulate immune evasion (*CD4/IL10*), cell death regulation (CASP1), and proliferative signaling (PIK3CA), confirming their dual role as prognostic biomarkers and potential treatment targets in AML.

Immuno-infiltration, also known as immune cell infiltration into the tumor microenvironment, plays a critical role in tumor growth and progression [37,38]. Immune components such as T cells, B cells, and NK cells can influence tumor behavior by directly recognizing and eliminating cancer cells, promoting an anti-tumor immune response, or promoting tumor cell growth and survival. Previous studies have reported that both the level and composition of immune infiltrates within tumors provide valuable prognostic and therapeutic insights across various cancer types, including AML [39–41]. Our study shows a significant difference in immune cell infiltration between high- and low-risk groups, further supporting the rationality of our prognostic model.

Changes in immune infiltration in high-risk AML patients reflect a profoundly immunosuppressive microenvironment that drives disease progression. Elevated M2 macrophages [42] and monocytes secrete IL-10 and TGF-β, suppressing cytotoxic T-cell activity and promoting leukemia stem cell maintenance [43]. Neutrophils in high-risk AML patients exhibit impaired neutrophil extracellular trap–associated cell death (NETosis), compromising infection defense while fostering pro-tumor inflammation [44]. Conversely, reduced NK cell infiltration results from AML-induced disruption of the bone marrow niche [45], which impairs innate tumor surveillance, and diminished regulatory T cells may disrupt immune homeostasis, paradoxically enabling unchecked leukemogenesis [46]. Together, these changes establish an immune-evasive niche that supports AML progression and therapy resistance, directly linking infiltration profiles to poor prognosis.

Previous studies have developed AML prognostic models based on ICD-related genes. For example, Chen *et al*. [7] constructed a five-gene ICD prognostic model (*TNF*, *CXCR3*, *CD4*, *PIK3CA*, *CALR*) and investigated immune infiltration, somatic mutations, and drug sensitivity. However, their study was limited to bioinformatics analyses, lacking experimental validation and mechanistic exploration of key genes. In contrast, our study presents a four-gene ICD prognostic model (*CD4*, *IL10*, *CASP1*, *PIK3CA*), which maintains predictive accuracy while reducing gene complexity and improving clinical relevance through experimental validation.

Unlike previous models, this study is the first to functionally validate CASP1, demonstrating its role in AML cell proliferation and chemoresistance, providing direct biological evidence for its prognostic significance. Additionally, this study incorporates the inflammatory marker C-reactive protein (CRP), offering a novel mechanistic link between ICD-related pathways and AML progression via inflammation and immune regulation. These advancements make the model more clinically applicable and mechanistically robust, addressing key limitations of previous bioinformatics-driven approaches.

However, the lack of validation in an independent cohort represents a limitation, potentially restricting the generalizability of our prognostic model across diverse AML populations. Future research should focus on validating this model using independent external cohorts, such as clinical datasets from other institutions or public databases like GEO, to confirm its robustness and applicability in varied clinical settings.

Conclusion

In summary, this study developed a prognostic model for AML incorporating four ICD-related genes (*CD4*, *IL10*, *CASP1*, and *PIK3CA*). The model demonstrates strong predictive accuracy and shows substantial association with immune cell infiltration, consistent with *in vitro* functional verification results. Further study should focus on validating this model using clinical samples to confirm its applicability and robustness.

Availability of Data and Materials

The datasets generated and analyzed during the current study are available from the corresponding author upon reasonable request.

Author Contributions

Substantial contributions to conception and design: GCL, YQG. Data acquisition, data analysis and interpretation: Both authors. Drafting the first version of the manuscript: GCL and YQG. Critical revision of the manuscript for important intellectual content: Both authors. Final approval of the version to be published: Both authors. Agreement to be accountable for all aspects of the work in ensuring that questions related to the accuracy or integrity of the work are appropriately investigated and resolved: Both authors.

Ethics Approval and Consent to Participate

Not applicable.

Acknowledgment

Not applicable.

Funding

This research received no external funding.

Conflict of Interest

The authors declare no conflict of interest.

Supplementary Material

Supplementary material associated with this article can be found, in the online version, at https://doi.org/10.24976/Discov.Med.202537200.162.

References

[1] Passaro D, Di Tullio A, Abarrategi A, Rouault-Pierre K, Foster K, Ariza-McNaughton L, *et al*. Increased Vascular Permeability in the Bone Marrow Microenvironment Contributes to Disease Progression and Drug Response in Acute Myeloid Leukemia. Cancer Cell. 2017; 32: 324–341.e6. https://doi.org/10.1016/j.ccell.2017.08.001.

[2] Brunetti L, Gundry MC, Sorcini D, Guzman AG, Huang YH, Ramabadran R, *et al*. Mutant NPM1 Maintains the Leukemic State through HOX Expression. Cancer Cell. 2018; 34: 499–512.e9. https://doi.org/10.1016/j.ccell.2018.08.005.

[3] Song Y, Tian S, Zhang P, Zhang N, Shen Y, Deng J. Construction and Validation of a Novel Ferroptosis-Related Prognostic Model for Acute Myeloid Leukemia. Frontiers in Genetics. 2022; 12: 708699. https://doi.org/10.3389/fgene.2021.708699.

[4] Kong W, He L, Zhu J, Brück O, Porkka K, Heckman CA, *et al*. An immunity and pyroptosis gene-pair signature predicts overall survival in acute myeloid leukemia. Leukemia. 2022; 36: 2384–2395. https://doi.org/10.1038/s41375-022-01662-6.

[5] Noren DP, Long BL, Norel R, Rrhissorrakrai K, Hess K, Hu CW, *et al*. A Crowdsourcing Approach to Developing and Assessing Prediction Algorithms for AML Prognosis. PLoS Computational Biology. 2016; 12: e1004890. https://doi.org/10.1371/journal.pcbi.1004890.

[6] Au KM, Balhorn R, Balhorn MC, Park SI, Wang AZ. High-Performance Concurrent Chemo-Immuno-Radiotherapy for the Treatment of Hematologic Cancer through Selective High-Affinity Ligand Antibody Mimic-Functionalized Doxorubicin-Encapsulated Nanoparticles. ACS Central Science. 2019; 5: 122–144. https://doi.org/10.1021/acscentsci.8b00746.

[7] Chen Y, Qiu X, Liu R. Comprehensive characterization of immunogenic cell death in acute myeloid leukemia revealing the association with prognosis and tumor immune microenvironment. BMC Medical Genomics. 2024; 17: 107. https://doi.org/10.1186/s12920-024-01876-w.

[8] Zhang J, Li H, Zhang X, Yang Y, Sun Y. The landscape of immunogenic cell death-related genes predicts the overall survival and immune infiltration status of non-small-cell lung carcinoma. Heliyon. 2025; 11: e40869. https://doi.org/10.1016/j.heliyon.2024.e40869.

[9] Li Y, Feng J, Wang T, Li M, Zhang H, Rong Z, *et al*. Construction of an immunogenic cell death-based risk score prognosis model in breast cancer. Frontiers in Genetics. 2022; 13: 1069921. https://doi.org/10.3389/fgene.2022.1069921.

[10] Jiao C, Ma X, Cui J, Su B, Xu F, Chen E, *et al*. Potential value of immunogenic cell death related-genes in refining European leukemiaNet guidelines classification and predicting the immune infiltration landscape in acute myeloid leukemia. Cancer Cell International. 2025; 25: 52. https://doi.org/10.1186/s12935-025-03670-9.

[11] Greiner J, Mohamed E, Fletcher DM, Schuler PJ, Schrezenmeier H, Götz M, *et al*. Immunotherapeutic Potential of Mutated NPM1 for the Treatment of Acute Myeloid Leukemia. Cancers. 2024; 16: 3443. https://doi.org/10.3390/cancers16203443.

[12] Tripodo C, Burocchi A, Piccaluga PP, Chiodoni C, Portararo P, Cappetti B, *et al*. Persistent Immune Stimulation Exacerbates Genetically Driven Myeloproliferative Disorders via Stromal Remodeling. Cancer Research. 2017; 77: 3685–3699. https://doi.org/10.1158/0008-5472.CAN-17-1098.

[13] Vivian J, Rao AA, Nothaft FA, Ketchum C, Armstrong J, Novak A, *et al*. Toil enables reproducible, open source, big biomedical data analyses. Nature Biotechnology. 2017; 35: 314–316. https://doi.org/10.1038/nbt.3772.

[14] Garg AD, De Ruysscher D, Agostinis P. Immunological metagene signatures derived from immunogenic cancer cell death associate with improved survival of patients with lung, breast or ovarian malignancies: A large-scale meta-analysis. Oncoimmunology. 2015; 5: e1069938. https://doi.org/10.1080/2162402X.2015.1069938.

[15] Meier P, Legrand AJ, Adam D, Silke J. Immunogenic cell death in cancer: targeting necroptosis to induce antitumour immunity. Nature Reviews. Cancer. 2024; 24: 299–315. https://doi.org/10.1038/s41568-024-00674-x.

[16] Galluzzi L, Guilbaud E, Schmidt D, Kroemer G, Marincola FM. Targeting immunogenic cell stress and death for cancer therapy. Nature Reviews. Drug Discovery. 2024; 23: 445–460. https://doi.org/10.1038/s41573-024-00920-9.

[17] Yoshihara K, Shahmoradgoli M, Martínez E, Vegesna R, Kim H, Torres-Garcia W, *et al*. Inferring tumour purity and stromal and immune cell admixture from expression data. Nature Communications. 2013; 4: 2612. https://doi.org/10.1038/ncomms3612.

[18] Ding PH, Yang MX, Wang NN, Jin LJ, Dong Y, Cai X, *et al*. *Porphyromonas gingivalis*-Induced NLRP3 Inflammasome Activation and Its Downstream Interleukin-1β Release Depend on Caspase-4. Frontiers in Microbiology. 2020; 11: 1881. https://doi.org/10.3389/fmicb.2020.01881.

[19] Döhner H, Estey E, Grimwade D, Amadori S, Appelbaum FR, Büchner T, *et al*. Diagnosis and management of AML in adults: 2017 ELN recommendations from an international expert panel. Blood. 2017; 129: 424–447. https://doi.org/10.1182/blood-2016-08-733196.

[20] DeNardo DG, Ruffell B. Macrophages as regulators of tumour immunity and immunotherapy. Nature Reviews. Immunology. 2019; 19: 369–382. https://doi.org/10.1038/s41577-019-0127-6.

[21] O'Donnell JS, Teng MWL, Smyth MJ. Cancer immunoediting and resistance to T cell-based immunotherapy. Nature Reviews. Clinical Oncology. 2019; 16: 151–167. https://doi.org/10.1038/s41571-018-0142-8.

[22] De Martino M, Rathmell JC, Galluzzi L, Vanpouille-Box C. Cancer cell metabolism and antitumour immunity. Nature Reviews. Immunology. 2024; 24: 654–669. https://doi.org/10.1038/s41577-024-01026-4.

[23] Padmakumar D, Chandraprabha VR, Gopinath P, Vimala Devi ART, Anitha GRJ, Sreelatha MM, *et al*. A concise review on the molecular genetics of acute myeloid leukemia. Leukemia Research. 2021; 111: 106727. https://doi.org/10.1016/j.leukres.2021.106727.

[24] Wen S, Lv X, Ma X, Deng S, Xie J, Yuan E. Immunogenic cell death (ICD) genes predict immunotherapy response and therapeutic targets in acute myeloid leukemia (AML). Frontiers in Genetics. 2024; 15: 1419819. https://doi.org/10.3389/fgene.2024.1419819.

[25] Dong C, Zhang N, Zhang L. The Multi-Omic Prognostic Model of Oxidative Stress-Related Genes in Acute Myeloid Leukemia. Frontiers in Genetics. 2021; 12: 722064. https://doi.org/10.3389/fgene.2021.722064.

[26] Min K, Lu C, Wu X, Zhong S, Ma P, Zheng Y, et al. Identifying an immunogenic cell death-related gene signature and HSPA6 infers adverse prognosis in acute myeloid leukemia. Journal of Cancer. 2025; 16: 3643–3653. https://doi.org/10.7150/jca.115717.

[27] Fu W, Ma G. Significance of immunogenic cell death-related genes in prognosis prediction and immune microenvironment landscape of patients with cutaneous melanoma. Frontiers in Genetics. 2022; 13: 988821. https://doi.org/10.3389/fgene.2022.988821.

[28] Guo RJ, Atenafu EG, Schimmer AD, Minden MD, Chang H. Expression of CD4 is correlated with an unfavorable prognosis in wild-type NPM1, FLT3-ITD-negative cytogenetically normal adult acute myeloid leukemia. International Journal of Laboratory Hematology. 2017; 39: 429–437. https://doi.org/10.1111/ijlh.12649.

[29] Wu X, Li S, Chen D, Zheng G, Zhang Z, Li Z, *et al*. An inflammatory response-related gene signature associated with immune status and prognosis of acute myeloid leukemia. American Journal of Translational Research. 2022; 14: 4898–4917.

[30] Gritsman K, Yuzugullu H, Von T, Yan H, Clayton L, Fritsch C, *et al*. Hematopoiesis and RAS-driven myeloid leukemia differentially require PI3K isoform p110α. The Journal of Clinical Investigation. 2014; 124: 1794–1809. https://doi.org/10.1172/JCI69927.

[31] Liu J, Zhao M, Feng X, Zeng Y, Lin D. Expression and prognosis analyses of CASP1 in acute myeloid leukemia. Aging. 2021; 13: 14088–14108. https://doi.org/10.18632/aging.203028.

[32] Wang Z, Pan L, Yu H, Wang Y. The long non-coding RNA SNHG5 regulates gefitinib resistance in lung adenocarcinoma cells by targetting *miR-377*/CASP1 axis. Bioscience Reports. 2018; 38: BSR20180400. https://doi.org/10.1042/BSR20180400.

[33] Thatikonda S, Chaudhary R, Meshkovska Y, Biernacki M, Slebos RJC, Song X, *et al*. PV-10 triggers immunogenic cell death in head and neck squamous cell carcinoma via endoplasmic reticulum stress and apoptosis. Molecular Cancer Therapeutics. 2025. https://doi.org/10.1158/1535-7163.MCT-24-0218. (online ahead of print)

[34] Sayitoglu EC, Luca BA, Boss AP, Thomas BC, Freeborn RA, Uyeda MJ, *et al*. AML/T cell interactomics uncover correlates of patient outcomes and the key role of ICAM1 in T cell killing of AML. Leukemia. 2024; 38: 1246–1255. https://doi.org/10.1038/s41375-024-02255-1.

[35] Chen N, Xu Y, Mou J, Rao Q, Xing H, Tian Z, *et al*. Targeting of IL-10R on acute myeloid leukemia blasts with chimeric antigen receptor-expressing T cells. Blood Cancer Journal. 2021; 11: 144. https://doi.org/10.1038/s41408-021-00536-x.

[36] Villaume MT, Arrate MP, Ramsey HE, Sunthankar KI, Jenkins MT, Moyo TK, *et al*. The delta isoform of phosphatidylinositol-3-kinase predominates in chronic myelomonocytic leukemia and can be targeted effectively with umbralisib and ruxolitinib. Experimental Hematology. 2021; 97: 57–65.e5. https://doi.org/10.1016/j.exphem.2021.02.008.

[37] Laumont CM, Banville AC, Gilardi M, Hollern DP, Nelson BH. Tumour-infiltrating B cells: immunological mechanisms, clinical impact and therapeutic opportunities. Nature Reviews. Cancer. 2022; 22: 414–430. https://doi.org/10.1038/s41568-022-00466-1.

[38] Mami-Chouaib F, Blanc C, Corgnac S, Hans S, Malenica I, Granier C, *et al*. Resident memory T cells, critical components in tumor immunology. Journal for Immunotherapy of Cancer. 2018; 6: 87. https://doi.org/10.1186/s40425-018-0399-6.

[39] Mao X, Xu J, Wang W, Liang C, Hua J, Liu J, *et al*. Crosstalk between cancer-associated fibroblasts and immune cells in the tumor microenvironment: new findings and future perspectives. Molecular Cancer. 2021; 20: 131. https://doi.org/10.1186/s12943-021-01428-1.

[40] Christofides A, Strauss L, Yeo A, Cao C, Charest A, Boussiotis VA. The complex role of tumor-infiltrating macrophages. Nature Immunology. 2022; 23: 1148–1156. https://doi.org/10.1038/s41590-022-01267-2.

[41] Vadakekolathu J, Minden MD, Hood T, Church SE, Reeder S, Altmann H, *et al*. Immune landscapes predict chemotherapy resistance and immunotherapy response in acute myeloid leukemia. Science Translational Medicine. 2020; 12: eaaz0463. https://doi.org/10.1126/scitranslmed.aaz0463.

[42] Xu ZJ, Gu Y, Wang CZ, Jin Y, Wen XM, Ma JC, *et al*. The M2 macrophage marker *CD206*: a novel prognostic indicator for acute myeloid leukemia. Oncoimmunology. 2019; 9: 1683347. https://doi.org/10.1080/2162402X.2019.1683347.

[43] Mondesir J, Ghisi M, Poillet L, Bossong RA, Kepp O, Kroemer G, *et al*. AMPK activation induces immunogenic cell death in AML. Blood Advances. 2023; 7: 7585–7596. https://doi.org/10.1182/bloodadvances.2022009444.

[44] Jiao C, Ma X, Cui J, Su B, Xu F, Chen E, *et al*. Potential value of immunogenic cell death related-genes in refining European leukemiaNet guidelines classification and predicting the immune infiltration landscape in acute myeloid leukemia. Cancer Cell International. 2025; 25: 52. https://doi.org/10.1186/s12935-025-03670-9.

[45] Sanz-Ortega L, Andersson A, Carlsten M. Harnessing up-regulated E-selectin while enhancing SDF-1α sensing redirects infused NK cells to the AML-perturbed bone marrow. Leukemia. 2024; 38: 579–589. https://doi.org/10.1038/s41375-023-02126-1.

[46] Song B, Lou J, Mu L, Lu X, Sun J, Tang B. An Innovative Telomere-associated Prognosis Model in AML: Predicting Immune Infiltration and Treatment Responsiveness. Current Medicinal Chemistry. 2024. https://doi.org/10.2174/0109298673334218241021044800. (online ahead of print)